

# Lawrence Berkeley National Laboratory

## LBL Publications

### Title

Influence of Nozzle Conditions and Discrete Forcing on the Developing Region of Turbulent Planar Jets

### Permalink

<https://escholarship.org/uc/item/13m2p6x7>

### Authors

Stanley, S A

Sarkar, S

### Publication Date

1999-04-01

### Copyright Information

This work is made available under the terms of a Creative Commons Attribution License, available at <https://creativecommons.org/licenses/by/4.0/>



# ERNEST ORLANDO LAWRENCE BERKELEY NATIONAL LABORATORY

## Influence of Nozzle Conditions and Discrete Forcing on the Developing Region of Turbulent Planar Jets

S.A. Stanley and S. Sarkar

National Energy Research  
Scientific Computing Division

April 1999

Submitted to  
*AIAA Journal*



REFERENCE COPY |  
Does Not |  
Circulate |  
Bldg. 50 Library - Ref.  
Lawrence Berkeley National Laboratory

## **DISCLAIMER**

This document was prepared as an account of work sponsored by the United States Government. While this document is believed to contain correct information, neither the United States Government nor any agency thereof, nor the Regents of the University of California, nor any of their employees, makes any warranty, express or implied, or assumes any legal responsibility for the accuracy, completeness, or usefulness of any information, apparatus, product, or process disclosed, or represents that its use would not infringe privately owned rights. Reference herein to any specific commercial product, process, or service by its trade name, trademark, manufacturer, or otherwise, does not necessarily constitute or imply its endorsement, recommendation, or favoring by the United States Government or any agency thereof, or the Regents of the University of California. The views and opinions of authors expressed herein do not necessarily state or reflect those of the United States Government or any agency thereof or the Regents of the University of California.

**Influence of Nozzle Conditions and Discrete Forcing on  
the Developing Region of Turbulent Planar Jets**

S.A. Stanley

National Energy Research Scientific Computing Division  
Ernest Orlando Lawrence Berkeley National Laboratory  
University of California  
Berkeley, California 94720

and

S. Sarkar

University of California, San Diego  
La Jolla, California 92093-0411

April 1999

# Influence of Nozzle Conditions and Discrete Forcing on the Developing Region of Turbulent Planar Jets \*

S. A. Stanley †

*Lawrence Berkeley National Laboratory, 50A-1148, Berkeley, CA 94720.*

S. Sarkar ‡

*University of California, San Diego, La Jolla, CA 92093-0411.*

April 26, 1999

## Abstract

Planar turbulent jets are of great interest in a broad range of engineering applications such as combustion, propulsion and environmental flows. The influence of the turbulence intensity at the inflow, the shear layer momentum thickness, as well as the effects of discrete forcing on the initial development of the jet are studied computationally. It is found that the inflow fluctuation intensity and shear layer momentum thickness have significant impact on the initial growth of the jet. Higher fluctuation intensity and thinner shear layers lead to more rapid growth of the jet with an asymptotic approach of the centerline turbulent kinetic energy to the self-similar values. The influence of the shear layer thickness suggests a strong dependence of the initial growth on the shear layer instabilities near the nozzle. Two-dimensional discrete forcing enhances the growth and two-dimensionality of the large-scale structures in the near field of the jet. However, significant three-dimensional small-scale structures coexist with the large-scale structures. The influence of the forcing is rapidly lost downstream as the large-scale structures break down.

## 1 Introduction

The flowfield near the nozzle in planar turbulent jets is initially dominated by the shear layers at the jet edges. Michalke and Freymuth [1] showed that near the nozzle lip, the most strongly growing disturbances are those corresponding to the shear layer. The shear layers spread downstream and interact to form a fully developed jet. Sato [2], Rockwell and Nicolls [3] as well as Antonia, *et al.* [4] showed that near the jet nozzle, the large-scale structures in the flowfield are predominately symmetric for flat exit velocity profiles. When the shear layers interact downstream these structures reorganize into an asymmetric configuration in the fully developed region of the jet. This reorganization as the flowfield develops from the shear layers near the nozzle to the fully developed jet downstream has a strong influence on the mixing in this region of the jet which is not well understood.

While the developing region of planar turbulent jets is of considerable engineering interest, most studies of turbulent plane jets have concentrated on the self-preserving region far downstream where the turbulence is fully developed. Bradbury [5], Gutmark and Wygnanski [6] and Ramaprian and

---

\*Presented in part as Paper 99-0288 at the AIAA 37th Aerospace Sciences Meeting, Reno, NV, Jan. 11-14, 1999.

†AIAA member.

‡Associate Professor, AIAA member.

Chandrasekhara [7], as well as numerous others, measured statistical quantities in the self-preserving region while Oler and Goldschmidt [8, 9], Antonia, *et al.* [4] and Mumford [10] studied the organization of the large-scale structures in the fully-developed region. Thomas and Goldschmidt [11, 12], Thomas and Chu [13] and Thomas and Prakash [14] are perhaps the only researchers to concentrate on the study of the transition from the shear layer dominated region near the nozzle to the fully-developed region of the jet downstream. In general, however, they concentrated on the spectral development and reorganization of the large-scale structures. Thomas and Goldschmidt identified both symmetric and asymmetric modes in the near field of the jet and suggest that the asymmetric modes are due to resonant forcing by the large-scale structures downstream. Thomas and Chu further confirmed the upstream feedback and suggest that it results from the loss of symmetry of the large-scale structures downstream of the end of the potential core. Finally, Thomas and Prakash studied the evolution from the shear layer modes near the nozzle to the jet column mode downstream in an “untuned” jet, where the subharmonic growth process in the shear layer is incapable of obtaining the jet mode,  $f_{jt}^* \neq f_{sl}^*/2^n$ .

Namer and Ötügen [15] performed a parametric study of the effects of Reynolds number on the initial development of the jet. They found that as the Reynolds number increases, the jet develops more rapidly in the near field. They also observe stronger overshoots in the downstream development of the centerline turbulence intensities for lower Reynolds number jets.

The purpose of this study is to characterize the influence of the jet nozzle conditions on the downstream evolution of the jet using direct numerical simulation, DNS. The effects of nozzle fluctuation intensity and shear layer momentum thickness on the jet growth, centerline mean velocity decay as well as centerline fluctuation intensity are discussed below. In addition, the influence of symmetric and antisymmetric forcing at discrete frequencies on the evolution of the near field of the jet is studied.

## 2 Numerical Techniques

The unsteady, compressible, Navier-Stokes equations for an ideal gas are solved in the following form. Conservation of mass,

$$\partial_t \rho + \partial_i (\rho u_i) = 0 \quad (1)$$

conservation of momentum,

$$\partial_t (\rho u_i) + \partial_j (\rho u_i u_j) = -\partial_i p + \frac{1}{Re} \partial_j \tau_{ij} \quad (2)$$

where,

$$\tau_{ij} = (\partial_j u_i + \partial_i u_j) - \frac{2}{3} \delta_{ij} \partial_k u_k \quad (3)$$

and the equation for conservation of energy written as an evolution equation for the pressure,

$$\partial_t p + u_i \partial_i p + \gamma p \partial_i u_i = \frac{\gamma}{Pr Re} \partial_i \partial_i T + \frac{\gamma - 1}{Re} \tau_{ij} \partial_i u_j \quad (4)$$

The Euler terms in these equations are marched in time using the low-storage, fourth-order Runge-Kutta integration scheme of Carpenter and Kennedy [16]. This low-storage scheme requires only one additional array for each flowfield variable, thus reducing the memory requirements relative to the classical Runge-Kutta scheme. In addition, this is a five-stage scheme for which the additional stage is added to increase the overall stability of the scheme. While this scheme does require an additional evaluation of the right-hand-side of the governing equations, the relaxed stability criteria makes the scheme 40% more efficient.

The viscous and conduction terms in equations 1–4 are evaluated using a first-order integration scheme. This is implemented by advancing the Euler terms as described above and then evaluating

and advancing the viscous and conduction terms with the first-order scheme. This technique requires 20% less computational work than advancing all of the terms using the Runge-Kutta scheme and has negligible impact on the results for the conditions of the jets in this study. The viscous and conduction terms are small compared to the advective terms and the Courant-Friedrichs-Lewy, CFL, criterion requires a time step small enough that first-order accuracy is sufficient.

A nonuniform fourth-order compact derivative scheme is utilized to evaluate the spatial derivatives. This scheme generalizes the uniform compact derivatives of Lele [17] to nonuniform meshes. This central derivative scheme is closed at the boundaries using inward biased, nonuniform, third-order compact derivatives based on the uniform derivatives of Carpenter, Gottlieb and Abarbanel [18]. The normal second-derivatives,  $\partial^2/\partial x^2$ ,  $\partial^2/\partial y^2$ , and  $\partial^2/\partial z^2$ , are evaluated using nonuniform, compact, second-derivative formulae while the cross derivative terms,  $\partial^2/\partial x\partial y$ , etc., are evaluated using two successive applications of the first-derivative formulae. This compact 3-4-3 derivative scheme allows the simulation of problems on an open, non-periodic, computational domain while maintaining an overall fourth-order accuracy on the nonuniform physical grid.

All finite difference schemes generate their largest errors at the highest wave numbers supported by the computational grid,  $\kappa_x = 1/(2\Delta x)$ . In order to eliminate these high wave number errors, a nonuniform fourth-order compact filter is utilized. As with the nonuniform derivatives, the nonuniform compact filters generalize the uniform filters of Lele [17] and provide fourth-order accuracy in the physical grid spacing  $\Delta x$ . This filter is tuned to significantly affect only wave numbers  $\kappa_x > 0.85/(2\Delta x)$  so that the filter does not remove dynamically significant scales of motion. All flowfield variables are filtered at the end of each time step.

One of the greatest difficulties in the simulation of spatially evolving flows is the formulation of the boundary conditions required for the open computational domain. In general, the flow occurs in an infinite or large physical domain, however in simulations it is required to truncate the domain to the region of interest. During this truncation, information about the flowfield is lost. At the inflow boundary, the governing equations are solved in a characteristic form. The time variation of the incoming characteristic variables are specified while the equation for the outgoing characteristic variable is solved using internal biased derivatives. This treatment of the inflow plane allows the jet to be forced with proper specification of the characteristic variables. In addition to this characteristic inflow forcing, a simple exponential damping term of the form

$$\partial_t(\rho u) = \text{Standard Terms} - \sigma(\rho u - \bar{\rho} \bar{u}) \quad (5)$$

is added to the streamwise momentum equation at the inflow plane. In this expression,  $\sigma = 0.22$  and  $\bar{\rho}$  and  $\bar{u}$  are the mean density and velocity profiles. These weak damping terms are added to neutralize the the long-time effects of the weak numerical diffusion, inherent in all high-order central difference schemes, on the inflow profiles. The weak damping terms coupled with the characteristic forcing provide steady mean profiles while allowing the desired fluctuation intensity about this mean.

For the downstream and sidewall boundaries, the nonreflecting boundary conditions of Thompson [19, 20] are used. The form of these conditions is allowed to switch between nonreflecting inflow and outflow at each point on the boundary based on the sign of the instantaneous local normal velocity. The corner points on the outflow boundary are treated as nonreflecting at an angle 45 degrees from the two adjacent boundaries. At all outflow points, the pressure correction terms of Rudy and Strikwerda [21] and later discussed by Poinso and Lele [22]

$$\lambda_{in} n_i \partial_i W_{in} = K(p - p_\infty) / \rho c \quad (6)$$

where,

$$K = \sigma c (1 - M_{max}^2) / L \quad (7)$$

are utilized in conjunction with the nonreflecting boundary conditions. In these expressions,  $n_i$  is the normal to the boundary,  $W_{in}$  is the incoming characteristic variable and  $\lambda_{in}$  is the propagation velocity.  $M_{max}$  is the maximum Mach number in the domain,  $L$  is a characteristic dimension of

the domain,  $c$  is the local speed-of-sound and the constant  $\sigma = 0.25$ . In the spanwise direction the domain is periodic.

In addition, a Perfectly Matched Layer, PML, buffer zone based on that of Hu [23] is utilized on the sidewall and downstream boundaries to further isolate the interior of the domain from the effects of the boundary conditions. In this technique a region is added at the boundary in which the grid is stretched in the normal direction. In this stretched region, exponential damping terms are added to the governing equations of the form (written for the density equation on a boundary whose normal is in the  $x$ -direction)

$$\partial_t \rho = \text{Standard Terms} - \sigma(x) (\rho - \bar{\rho}) \quad (8)$$

where,

$$\sigma(x) = \sigma_m \left( \frac{x - x^*}{L_b} \right)^\beta \quad (9)$$

In these expressions,  $x^*$  is the location of the interface between the buffer zone and the domain interior and  $L_b = x_{max} - x^*$  is the length of the buffer zone. This term acts to damp the density to the specified value,  $\bar{\rho}$ , across the buffer zone. Constant values of  $\sigma_m = 2.0$  and  $\beta = 2.0$  are used on all three nonreflecting boundaries. On the sidewall boundaries, the streamwise velocity is damped to the co-flow velocity while on the outflow boundary the streamwise velocity was damped to the profile of Bradbury [5]

$$\frac{U - U_2}{\Delta U_c} = \exp[-0.6749\eta^2 (1.0 + 0.027\eta^4)] \quad (10)$$

where  $\eta = y/\delta_U$  and  $\Delta U_c = U(y=0) - U_2$  is the centerline velocity excess. A target jet growth rate of  $\delta_U/h = 0.1235(x/h - 0.873)$  is used. The lateral velocity is damped to the profile given by the requirement that the mean field remain divergence free,  $\partial_i U_i = 0.0$  on the outflow boundary and to zero on the sidewall boundaries. The value of the centerline velocity excess,  $\Delta U_c$ , in the outflow buffer zone is selected to maintain the same excess momentum flux

$$J = \rho \int_{-\infty}^{\infty} U(U - U_2) dy \quad (11)$$

at the outflow plane as was present at the inflow. The spanwise velocity is damped to zero on all boundaries and the pressure and density are damped to the constant inflow conditions. The grid stretching in the buffer zones is given by a simple geometric progression with a 5% stretching ratio.

The mean streamwise velocity profiles in the shear layers on either side of the jet at the inflow are given by a hyperbolic tangent profile,

$$u = \frac{U_1 + U_2}{2} + \frac{U_1 - U_2}{2} \tanh[y/(2\theta_o)] \quad (12)$$

where  $\theta_o$  is the shear layer momentum thickness, while  $U_1$  and  $U_2$  are the velocities of the high- and low-speed streams, respectively. This profile is mirrored across the centerline to obtain a top-hat profile with smooth edges. The mean lateral and spanwise velocities are zero at the inflow. The mean pressure and density profiles are uniform initially, however a small variation across the jet is generated due to the outgoing acoustic.

Two types of forcing are utilized in the simulations discussed herein, broadband and discrete. The broadband forcing is designed to provide energy to the flowfield in a range of scales characteristic of those present in an actual turbulent flow in order to increase the rate at which the jet evolves from the top-hat profiles present at the inflow to self-similar profiles downstream. This broadband forcing is performed by generating a volume of data with a three-dimensional energy spectrum given by

$$E(\kappa) = \frac{\kappa^4}{16} \exp\left[-2\left(\frac{\kappa}{\kappa_o}\right)^2\right] \quad (13)$$



Table 1: Inflow parameters.

| Case | $\theta/h$ | $q_{bb}/\Delta U$ | $q_{disc}/\Delta U$ |
|------|------------|-------------------|---------------------|
| A    | 0.05       | 0.10              | 0.0                 |
| B    | 0.05       | 0.05              | 0.0                 |
| C    | 0.05       | 0.025             | 0.0                 |
| D    | 0.09       | 0.05              | 0.0                 |
| E    | 0.025      | 0.05              | 0.0                 |
| F    | 0.05       | 0.05              | 0.02 (Symm.)        |
| G    | 0.05       | 0.05              | 0.02 (Asymm.)       |

and a profile across the jet such that the fluctuation intensity peaks in the shear layers. This velocity field is generated to be divergence free. The corresponding pressure field is calculated by solving  $\partial_k \partial_k p = -\rho \partial_j u_i \partial_i u_j$  and the density is specified by  $\rho = p/c^2$  where  $c$  is the mean speed-of-sound. By calculating the density fluctuations in this way, the production of entropy at the inflow is reduced. This box of data is then convected past the inflow plane as the solution is integrated in time using a constant convection velocity,  $U_c = (U_1 + U_2)/2$ . A sixth degree interpolating polynomial is utilized to obtain the velocity, pressure and density fields which are then used to calculate the incoming characteristic variables. Forcing the inflow with a finite length time series in this way introduces a low frequency component due to the periodicity of the inflow data. However, with a carefully designed time series, such that the periodic frequency at the inflow is far from the dominant frequencies in the flowfield, this has minimal effect.

The discrete perturbations are added to the inflow forcing using analytic formulae for divergence free perturbation velocities consisting of a combination of sines and cosines. The discrete forcing in the cases discussed below is purely two-dimensional and includes energy in the most unstable and first subharmonic mode from the linear-stability analysis of the hyperbolic tangent shear layers on either side of the jet. A phase shift of  $\pi/2$  is imposed between the fundamental and subharmonic modes.

The computational grid used in this study are generated using a simple geometric progression,  $\Delta y_{i+1} = \Lambda_i \Delta y_i$ . In the streamwise,  $x$ , direction, the grid is uniform everywhere except in the buffer zone at the outflow. In the lateral,  $y$ , direction the grid is uniform in the region  $-4.0h < y < 4.0h$  around the core of the jet where  $h$  is the jet nozzle width at the inflow plane. In the spanwise,  $z$ , direction the grid is uniform throughout.

### 3 Results and Discussion

The variation of the physical parameters for the simulations discussed herein is given in Table 1. All of these simulations are at a jet Reynolds number,  $Re_h = \rho h \Delta U / \mu = 3000$  and a convective Mach number,  $M_c = \Delta U / (c_1 + c_2) = 0.16$ . While these simulations are performed using the compressible Navier-Stokes equations, they are essentially incompressible due to the low convective Mach number. The velocity ratio,  $\eta = \Delta U / (U_1 + U_2)$  is 0.83 and the Prandtl number,  $Pr = C_p \mu / k = 0.72$ .

All of the calculations in this study are performed on a grid of physical dimensions,  $L_x = 13.5h + 1.6h$ ,  $L_y = 13.4h + 2.8h$  and  $L_z = 4h$  where  $h$  is the jet nozzle width. For all cases except *E* the computational grid is  $205 \times 189 \times 60$  and the grid spacing in the interior of the computational domain is  $\Delta x = \Delta y = \Delta z = 0.066h$ . For case *E* the computational domain is  $205 \times 277 \times 60$  and the grid spacing is  $\Delta x = \Delta z = 0.066h$  and  $\Delta y = 0.033h$ . The finer grid spacing in the  $y$ -direction is required to resolve the shear layer near the nozzle in this simulation.

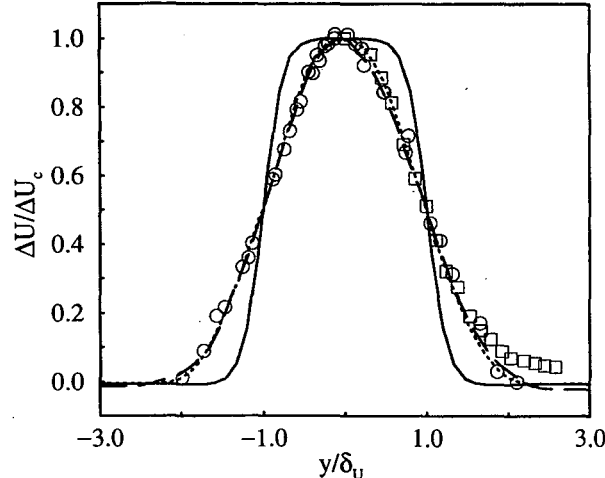


Figure 1: Mean streamwise velocity profiles, case A. —  $x/h = 0.0$ , .....  $x/h = 4.0$ , ---  $x/h = 11.5$ , □ Gutmark and Wygnanski [6], ○ Ramaprian and Chandrasekhara [7].

### 3.1 Comparison with Experimental Data

Figure 1 shows the mean streamwise velocity profiles at several downstream stations for case A compared against the experimental data of Gutmark and Wygnanski[6] and Ramaprian and Chandrasekhara[7]. The sharp initial shear layer profiles can be seen for the station  $x = 0.0h$ . For this case, the mean streamwise velocity profiles exhibit self-similarity for stations downstream of  $x = 4.0h$ . This station is very near the point at which the two shear layers on either side of the jet first merge. As can be seen, good comparison with experimental data for turbulent plane jets is observed.

Analysis of the self-similar region of planar turbulent jets predicts a linear relationship between the jet half-width,  $\delta_U$ , and the downstream coordinate,  $x$ ,

$$\frac{\delta_U}{h} = K_{1u} \left[ \frac{x}{h} + K_{2u} \right] \quad (14)$$

For case A the constants in this relationship are  $K_{1u} = 0.094$  and  $K_{2u} = 0.904$ . The growth rates,  $K_{1u}$ , are a little low compared to the values of 0.100 of Gutmark and Wygnanski and 0.110 from Ramaprian and Chandrasekhara. In general, there is a great deal of scatter in the virtual origins,  $K_{2u}$ . Ramaprian and Chandrasekhara reported a virtual origin of  $-1.0$  while Gutmark and Wygnanski reported  $-2.0$ . However, values for the virtual origin ranging from  $-5.0$  (Browne, *et al.* [24]) to 2.16 (Hussain and Clarke [25]) have been reported experimentally. These values are extremely sensitive to inflow conditions as will be discussed below.

Analysis of the self-similar centerline velocity decay predicts an inverse-squared relationship between the centerline velocity excess,  $\Delta U_c$ , and the downstream coordinate,  $x$ ,

$$\left( \frac{\Delta U_o}{\Delta U_c} \right)^2 = C_{1u} \left[ \frac{x}{h} + C_{2u} \right] \quad (15)$$

where  $\Delta U_o$  is the centerline velocity excess at the jet nozzle. The constants in this expression for case A are  $C_{1u} = 0.208$  and  $C_{2u} = -0.577$ . The centerline velocity decay rate,  $C_{1u}$ , compares relatively well with the experimentally observed values ranging from 0.093 (Ramaprian and Chandrasekhara [7]) to 0.220 (Thomas and Chu [13], Thomas and Prakash [14]). The value of Ramaprian and Chandrasekhara is lower than other observed values. However, they found that by using a scaling that accounts for variations in the conservation of streamwise momentum, the range of the

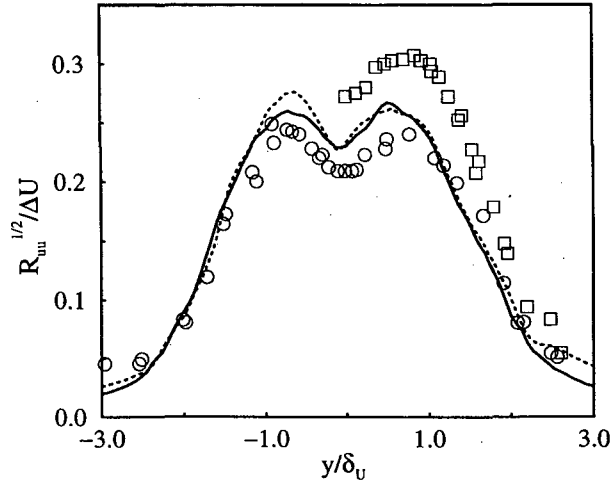


Figure 2: Streamwise Reynolds stress profiles, case A. —  $x/h = 10.0$ , - - -  $x/h = 11.5$ ,  $\square$  Gutmark and Wygnanski [6],  $\circ$  Ramaprian and Chandrasekhara [7].

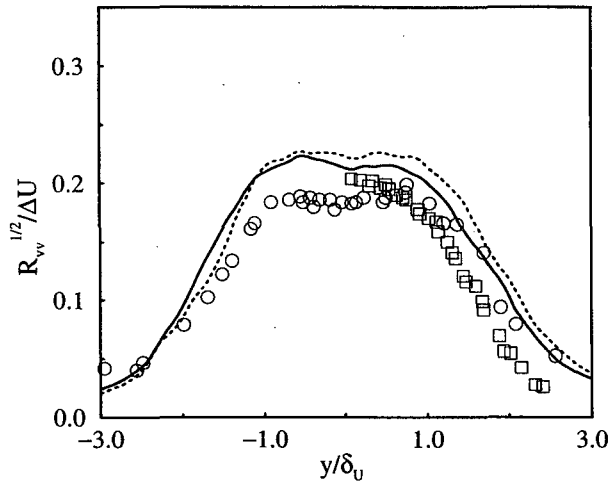


Figure 3: Lateral Reynolds stress profiles, case A. —  $x/h = 10.0$ , - - -  $x/h = 11.5$ ,  $\square$  Gutmark and Wygnanski [6],  $\circ$  Ramaprian and Chandrasekhara [7].

centerline velocity decay rates from different experimental studies was reduced. Using the scaling suggested by Ramaprian and Chandrasekhara, their value for  $C_{1u}$  becomes 0.168 while the value for the current DNS is 0.183. Unfortunately, insufficient data is available to calculate the adjusted values from Thomas and Chu and Thomas and Prakash. These corrections have insignificant effects on the jet growth rates and virtual origins.

For brevity, only a limited comparison of these results against experimental data is discussed here. For a more detailed analysis of a single simulation, as well as a more complete comparison with the available experimental data see Stanley and Sarkar [26, 27].

### 3.2 Influence of the Inflow Fluctuation Intensity

In most experimental studies, the fluctuation intensity at the jet nozzle is only reported on the centerline. However, due to the boundary layers upstream, the fluctuation intensity peaks in the shear layers on either side of the jet. Since the peak mean shear is also in the shear layers near the

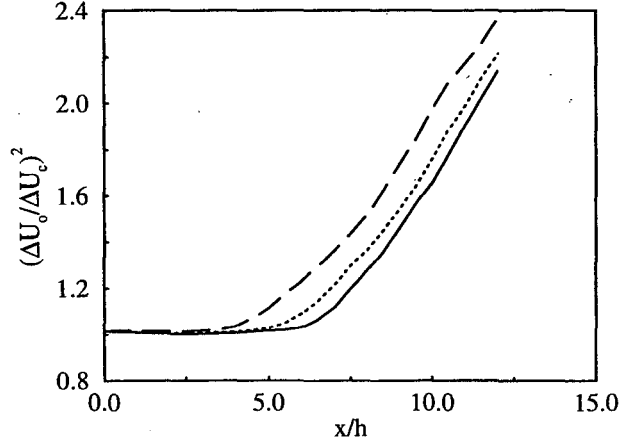


Figure 4: Downstream evolution of the centerline velocity excess for different broadband inflow intensities. —  $q/\Delta U = 0.025$ , .....  $q/\Delta U = 0.05$ , ---  $q/\Delta U = 0.10$

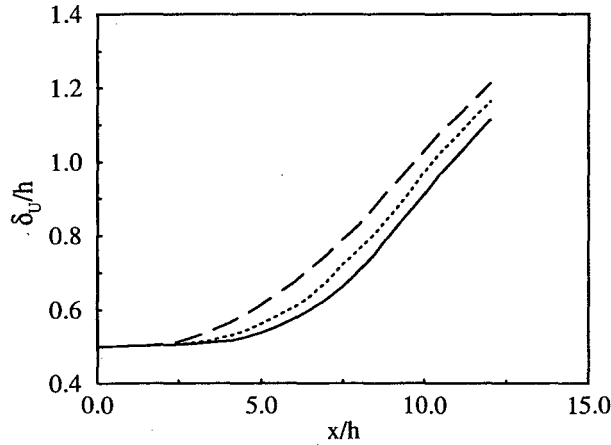


Figure 5: Downstream evolution of the jet half-width for different broadband inflow intensities. —  $q/\Delta U = 0.025$ , .....  $q/\Delta U = 0.05$ , ---  $q/\Delta U = 0.10$

nozzle, it is clear that the fluctuation intensity in this region of the jet will have a strong influence on the initial downstream evolution. In order to characterize the influence of the fluctuation intensity on the initial development of planar jets, results from three simulations, cases *A*, *B* and *C*, with different broadband intensities at the inflow plane are presented. It is believed that the broadband intensity in case *C* is relatively typical of that in experimental studies with laminar boundary layers while the broadband intensity in case *A* is closer to that which would occur in a jet exiting from a turbulent channel.

Figures 4 and 5 show the variation with broadband inflow forcing intensity of the evolution of the centerline mean velocity excess and the jet half-width, respectively. It is clear from these figures that the inflow fluctuation intensity has a strong influence on the initial growth of the jet. When the inflow fluctuation intensity is increased from  $q_{bb}/\Delta U_c = 0.025$  to 0.10 the length of the potential core, based on the constancy of the centerline mean velocity excess, decreases from  $6h$  to  $3h$ . However, in the self-similar region downstream, the jet grows at nearly the same rate and the centerline velocity excess decays at nearly the same rate for all inflow fluctuation intensities.

Table 2 gives the parameters for the self-similar fits of the jet half-width and the centerline mean velocity excess for all three cases. It can be seen that there is a strong increase in the magnitude

Table 2: Variation of the jet growth and centerline velocity decay coefficients with inflow fluctuation intensity.

| Case | $q_{bb}/\Delta U$ | $K_{1u}$ | $K_{2u}$ | $C_{1u}$ | $C_{2u}$ |
|------|-------------------|----------|----------|----------|----------|
| A    | 0.10              | 0.094    | 0.904    | 0.212    | -0.760   |
| B    | 0.05              | 0.100    | -0.280   | 0.216    | -1.78    |
| C    | 0.025             | 0.102    | -1.02    | 0.228    | -2.64    |

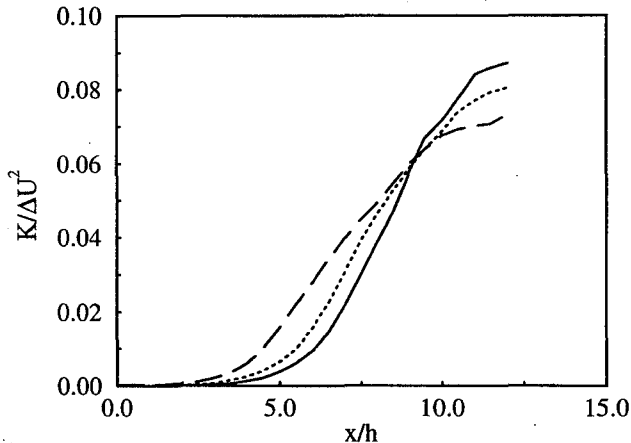


Figure 6: Downstream evolution of the centerline turbulence intensity for different broadband inflow intensities. —  $q/\Delta U = 0.025$ , .....  $q/\Delta U = 0.05$ , - -  $q/\Delta U = 0.10$

of the virtual origins,  $K_{2u}$  and  $C_{2u}$ , for increasing inflow fluctuation intensity. There is also a slight decrease in the jet growth rates,  $K_{1u}$ , and centerline velocity decay rates,  $C_{1u}$ . While this change is small, it is consistent across the range of  $q_{bb}/\Delta U_c$  studied. It is likely that this variation is a result of the focus on the developing region of the jet and that self-similar fits further downstream would show less influence of the nozzle conditions.

Figure 6 shows the variation of the downstream growth of the centerline turbulent kinetic energy with changes in the inflow fluctuation intensity. As expected, the initial growth of the centerline turbulent kinetic energy is more rapid for the highest inflow fluctuation intensity than for the smallest. The region of strong growth in the turbulent kinetic energy shifts from  $\approx 3.5h$  to  $\approx 7.0h$  with a decrease in the broadband forcing intensity from 0.10 to 0.025. However, near the outflow of the domain, the centerline turbulent kinetic energy for the cases with lower intensity inflow fluctuations exceeds the turbulent kinetic energy for the highest inflow fluctuation intensity. For  $q_{bb}/\Delta U_c = 0.10$  the centerline turbulent kinetic energy,  $K/\Delta U^2$ , grows asymptotically to a value  $\approx 0.07$ . Gutmark and Wagnanski [6] observed a centerline turbulent kinetic energy of 0.075 while Browne, *et al.* [24] found 0.05. However for lower intensity fluctuations at the inflow, the centerline turbulent kinetic energy overshoots to values of 0.08 and 0.09 in the DNS. With a longer computational domain, it is speculated that a slow decay would be observed downstream to the values more typical of turbulent planar jets.

Figure 7 shows the downstream evolution of the ratio of the turbulent kinetic energy,  $K$ , to the dissipation,  $\epsilon$ , on the jet centerline for these three simulations. The evolution of this ratio is an indicator of the relative state of equilibrium of the turbulence. It can be seen that near the inflow this ratio is large, small dissipation relative to the turbulent kinetic energy, indicating that the turbulence is highly non-equilibrium. Downstream, the dissipation grows relative to the turbulent kinetic energy and this ratio approaches a value of  $\approx 6.5$  for all three inflow fluctuation

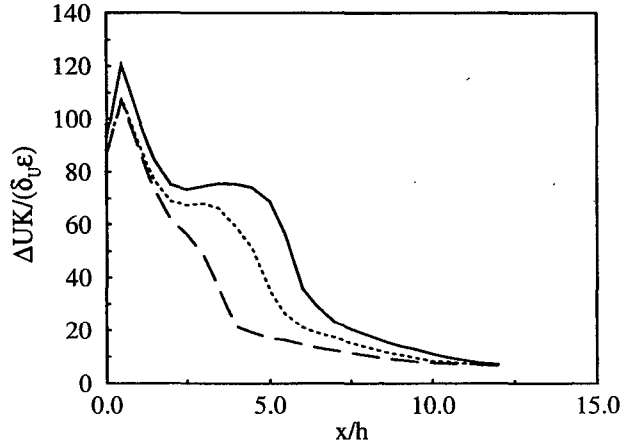


Figure 7: Downstream evolution of the turbulent kinetic energy to dissipation ratio on the jet centerline for different broadband inflow intensities. —  $q/\Delta U = 0.025$ , .....  $q/\Delta U = 0.05$ , ---  $q/\Delta U = 0.10$

intensities. For  $q_{bb}/\Delta U = 0.10$ , the turbulent fields approach equilibrium quickly downstream in the jet as indicated by the rapid approach of  $\Delta UK/(\delta_U \epsilon)$  to the equilibrium value. However, for the lower inflow fluctuation intensities, the development of equilibrium turbulence is slower. This relatively larger region of non-equilibrium turbulence for smaller inflow fluctuation intensities allows the overshoot in the turbulent kinetic energy downstream in the jet.

Similar overshoots in the turbulent kinetic energy were observed by Namer and Ötügen [15] and Browne, *et al.* [24]. Namer and Ötügen also observed an influence of the jet Reynolds number on the overshoot in the turbulence intensities. They found that jets with lower initial Reynolds numbers,  $Re_h$ , developed larger overshoots in the centerline streamwise fluctuation intensity. A large overshoot was observed for a  $Re_h = 1000$  jet while for  $Re_h = 7000$ , no overshoot was observed in the streamwise fluctuation intensity.

### 3.3 Influence of the Shear Layer Momentum Thickness

The momentum thickness of the shear layers at the jet nozzle are often quoted in studies of planar jets. However, no consistent study of the influence of the initial shear layer thickness on the development of the jet has been performed. In order to understand the influence of the initial momentum thickness, three simulations have been performed with varying shear layer thickness. Cases *D*, *B* and *E* have initial momentum thicknesses,  $\theta_o$ , of  $0.09h$ ,  $0.05h$  and  $0.025h$ , respectively. The initial fluctuation intensity for all of these cases is  $q_{bb}/\Delta U = 0.05$ .

Figures 8 and 9 show the effect of varying the shear layer momentum thickness on the centerline mean excess velocity decay and the jet half-width. While the shear layer conditions are often ignored when comparing the evolution of jets from different studies, the current results demonstrate unequivocally that the shear layer momentum thickness is an important parameter in the characterization of the initial region of planar turbulent jets. When the shear layer momentum thickness decreases from  $0.09h$  to  $0.025h$ , the length of the potential core of the jet based on the constancy of the centerline mean velocity excess decreases from  $6.0h$  to  $3.5h$ . Likewise, there is a strong shift in the location at which the jet width grows strongly from  $6.0h$  to  $2.0h$ .

As shown above for the inflow intensity, the decrease in the shear layer momentum thickness is most strongly felt in the virtual origins in the self-similar fits of the jet half-width and the centerline velocity decay, Table 3. There is a strong increase in the virtual origins,  $K_{2u}$  and  $C_{2u}$ , with a decrease in the momentum thickness. There is also a significant influence of the inflow momentum

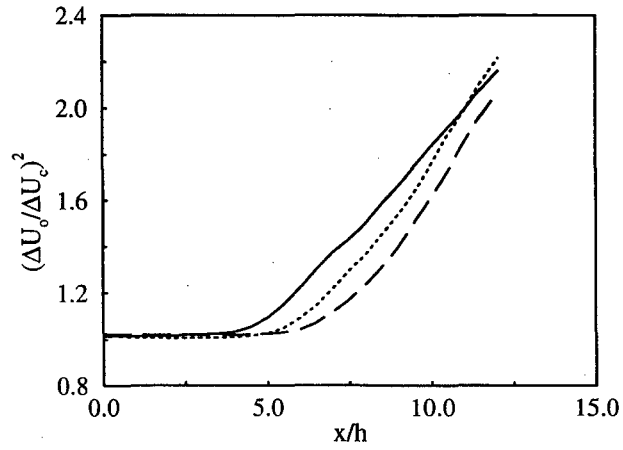


Figure 8: Downstream evolution of the centerline velocity excess for different initial shear layer momentum thicknesses. —  $\theta_o/h = 0.025$ , .....  $\theta_o/h = 0.05$ , --  $\theta_o/h = 0.09$

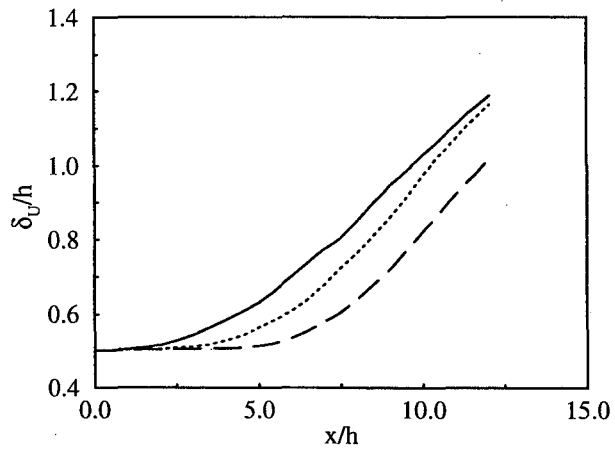


Figure 9: Downstream evolution of the jet half-width for different initial shear layer momentum thicknesses. —  $\theta_o/h = 0.025$ , .....  $\theta_o/h = 0.05$ , --  $\theta_o/h = 0.09$

Table 3: Variation of the jet growth and centerline velocity decay coefficients with initial shear layer momentum thickness.

| Case | $\theta_o/h$ | $K_{1u}$ | $K_{2u}$ | $C_{1u}$ | $C_{2u}$ |
|------|--------------|----------|----------|----------|----------|
| D    | 0.09         | 0.098    | -1.66    | 0.224    | -2.74    |
| B    | 0.05         | 0.100    | -0.280   | 0.216    | -1.78    |
| E    | 0.025        | 0.082    | 2.44     | 0.160    | 1.47     |

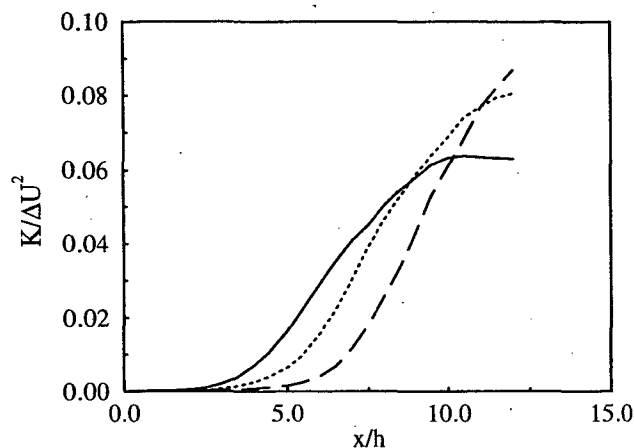


Figure 10: Downstream evolution of the centerline turbulence intensity for different initial shear layer momentum thicknesses. —  $\theta_o/h = 0.025$ , .....  $\theta_o/h = 0.05$ , - -  $\theta_o/h = 0.09$

thickness on the jet growth rates,  $K_{1u}$ , and centerline velocity decay rates,  $C_{1u}$ . There is an 18% change in the jet growth rates and a 28% change in the centerline velocity decay rates over the range of momentum thickness studied. In contrast, there is only an 8% change in the growth rates and velocity decay rates for the range of inflow forcing intensity discussed above. While the change in the centerline velocity decay rate is consistent across the range of momentum thickness, the change in the jet growth rate is not. Again, it is likely that this influence of the nozzle conditions on the downstream growth and centerline velocity decay rates is a result of the focus on the developing region of the jet.

Figure 10 shows the downstream evolution of the centerline turbulent kinetic energy for the three simulations. Decreasing the shear layer momentum thickness has a similar influence on the centerline turbulent kinetic energy as the increase in the inflow fluctuation intensity discussed above. As the shear layer momentum thickness is decreased, the region of strong growth in the turbulent kinetic energy shifts towards the nozzle from  $\approx 6.0h$  to  $\approx 3.0h$ . For the smallest shear layer thickness, the centerline turbulent kinetic energy grows very strongly and asymptotes rapidly to a value of 0.06. For the thicker shear layers, the growth in the turbulent kinetic energy is slower and an overshoot, with respect to self-similar values reported in experiments and observed in the DNS with  $\theta_o/h = 0.025$ , occurs near the outflow of the domain.

As above, the asymptotic growth of the centerline turbulent kinetic energy for  $\theta_o/h = 0.025$ , while an overshoot occurs for the thicker initial shear layers, can be related to the rate at which the turbulence approaches an equilibrium state downstream. Figure 11 shows the downstream evolution of the ratio of the turbulent kinetic energy to the dissipation for the jets with differing inflow shear layer thicknesses. Again, near the inflow the turbulence is highly non-equilibrium. For  $\theta_o/h = 0.025$  the fluctuating velocity fields rapidly develop to equilibrium turbulence while for the thicker initial shear layers this evolution is slower. The difference in the evolution of the turbulent fields to



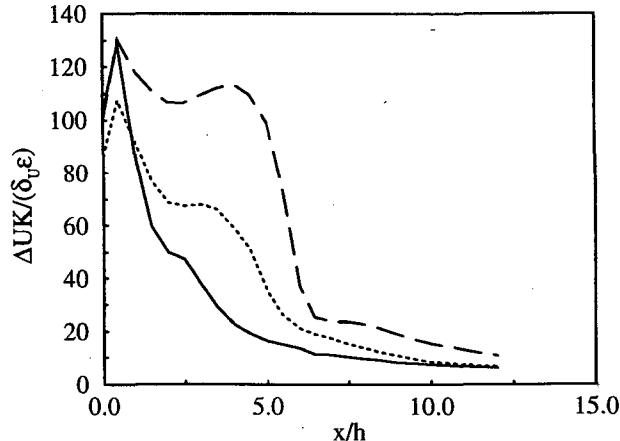


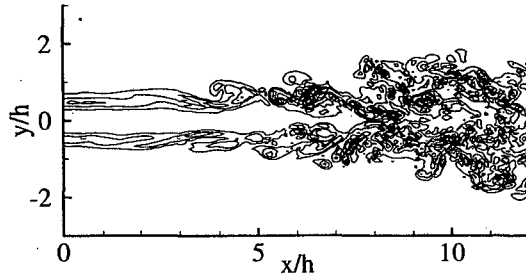
Figure 11: Downstream evolution of the turbulent kinetic energy to dissipation ratio on the jet centerline for different initial shear layer momentum thicknesses. —  $\theta_o/h = 0.025$ , .....  $\theta_o/h = 0.05$ , - -  $\theta_o/h = 0.09$

equilibrium for a change in the inflow momentum thickness is more dramatic than was observed earlier for variations in the inflow fluctuation intensity. For  $\theta_o/h = 0.09$  the fluctuating fields remain highly non-equilibrium until downstream of  $x \approx 6.0h$  where there is a very rapid increase in the dissipation relative to the turbulent kinetic energy, decrease in  $\Delta UK/(\delta_U \epsilon)$ . This is followed by a much slower approach downstream to equilibrium turbulence. This slow approach to equilibrium allows a large overshoot in the turbulent kinetic energy downstream in this jet relative to the jet with  $\theta_o/h = 0.025$ .

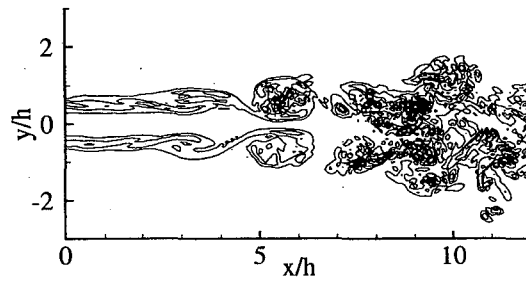
### 3.4 Influence of Discrete Forcing on the Jet Development

This section discusses the influence of forcing the jet inflow plane using discrete forcing at the shear layer fundamental and first subharmonic frequencies. Forcing at frequencies associated with the shear layers, rather than the downstream jet mode, is utilized since the experimental work of Michalke and Freymuth [1] show that the strongest growing modes near the nozzle in natural developing planar jets are those of the shear layer. However, it would be of interest to perform comparisons with forcing at the jet mode as well. The two discretely forced cases, *F* and *G*, include a broadband forcing at the inflow plane with an intensity of  $q_{bb}/\Delta U_c = 0.05$  superimposed with the two-dimensional discrete forcing with  $q_{disc}/\Delta U_c = 0.02$ , Table 1. Case *F* is forced symmetrically with respect to the centerline while case *G* is forced asymmetrically. While the broadband intensity is larger, the energy is spread across a large range of scales. The energy in the discrete forcing, on the other hand, is concentrated at only two frequencies and provides roughly an order of magnitude larger energy in these modes than is present in the broadband spectrum at the same frequencies.

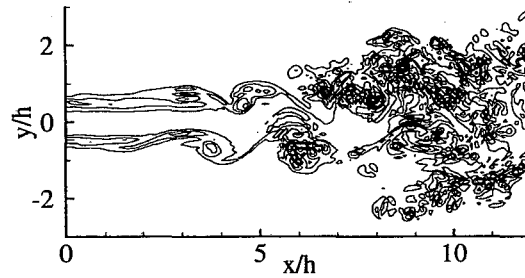
Figures 12(a) and 13(a) show the spanwise vorticity contours on an  $x/y$ -plane ( $z = 0.0h$ ) and an  $x/z$ -plane ( $y = 0.5h$ ), respectively, for case *A*. This case has no discrete forcing and serves as the unforced reference for the two discretely forced cases. For this simulation, there are no “strong” large scale structures in the flowfield near the nozzle. For simulations with broadband inflow conditions, the strongest growing mode near the jet nozzle is the shear layer mode (see Stanley and Sarkar [26]). However, there is a rapid growth in the energy at all scales due to nonlinear interactions and no strong large-scale structures appear in the visualization. The lack of contour lines at  $x = 0.0h$  in Figure 13(a) indicate that the spanwise vorticity contours are relatively two-dimensional near the jet nozzle. However, there is a rapid increase in the three-dimensionality downstream. By  $x = 5.0h$  strong small-scale, three-dimensional, structures are present in the flowfield.



(a) Broadband forcing only.

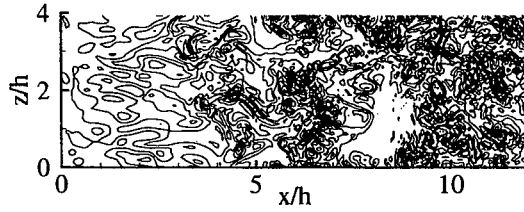


(b) Symmetric discrete forcing.

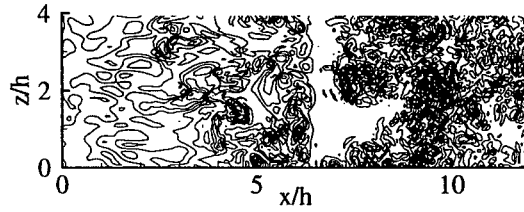


(c) Asymmetric discrete forcing.

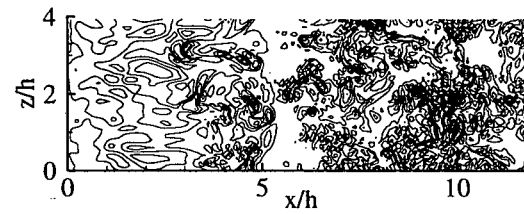
Figure 12: Spanwise vorticity contours on an  $x/y$ -plane ( $z = 0.0h$ ).



(a) Broadband forcing only.



(b) Symmetric discrete forcing.



(c) Asymmetric discrete forcing.

Figure 13: Spanwise vorticity contours on an  $x/z$ -plane in the upper shear layer, ( $y = 0.5h$ ).

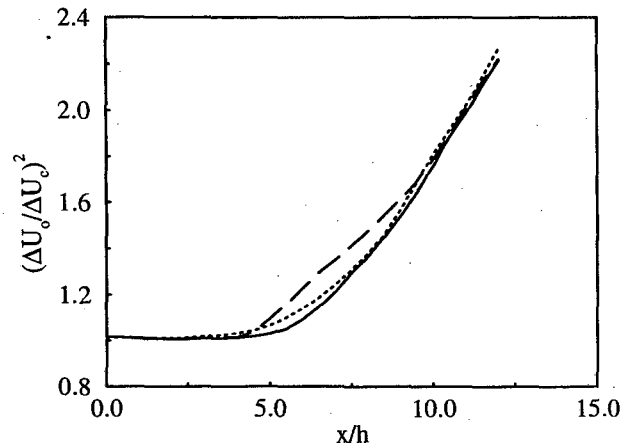


Figure 14: Downstream evolution of the centerline velocity excess for discretely forced jets. — Unforced, ..... Symmetrically forced, --- Asymmetrically forced.

Figures 12(b) and 12(c) show the spanwise vorticity contours on an  $x/y$ -plane for the symmetrically and asymmetrically forced planar jet simulations, respectively. While the large-scale structures did not show strongly in the visualization of the vorticity field for the unforced case, for the discretely forced simulations the large-scale structures are very evident. In case  $F$ , strong symmetrically oriented structures are present in the flowfield in the region  $3.0h \leq x \leq 7.0h$ , while in case  $G$  the structures are arranged asymmetrically. It is interesting to note that accompanying the large-scale structures in both simulations there exists a great deal of small-scale three-dimensional structures. Downstream in the jets,  $x > 7.0h$ , there is a strong breakdown of the large-scale structures to small-scale turbulence in both forced simulations.

Figures 13(b) and 13(c) show the spanwise vorticity contours on an  $x/z$ -plane in the upper shear layer for the two discretely forced simulations. While there is considerable three-dimensionality on the smaller-scales, the large-scale structures present in the region  $3.0h \leq x \leq 7.0h$  are strongly two-dimensional (indicated by the sharp break between the region of high vorticity and low vorticity at  $x = 6.0h$  for all values of  $z$ ). This is a result of the fact that the discrete forcing at the inflow plane is two-dimensional. In Figure 13(b), small-scale three-dimensional structures present within the two-dimensional large-scale vortical structure can be seen in the region  $5.0h \leq x \leq 6.0h$ . In this region, the  $x/z$ -slice in Figure 13(b) passes thorough the large-scale structure in the upper half of the jet. The breakdown of the two-dimensional large-scale structures downstream is evident in Figure 13(b) by the lack of two-dimensionality for  $x > 6.0h$ . In the region downstream, the strong growth in the three-dimensional small-scale turbulent structures overwhelms the two-dimensional forcing at the inflow.

Figures 14 and 15 show the downstream evolution of the centerline velocity decay and the jet half-width for the two discretely forced jets as well as the unforced reference. While the discrete forcing does influence the jet growth and centerline velocity decay in the region  $3.0h \leq x \leq 10.0h$ , the effect is relatively small. The strongest effect is observed in the asymmetrically forced jet. Downstream,  $x > 10.0h$ , the jet half-width and centerline velocity excess collapse with that of the unforced jet. For the symmetrically forced jet, case  $F$ , the effect of forcing is smaller and the collapse to the unforced behavior occurs more rapidly. Thus, discrete forcing influences the mean fields in the region near the jet nozzle, however downstream the mean field does not feel the effect of the inflow forcing.

While discrete forcing has little influence on the mean streamwise velocity field downstream, it is evident from Figure 12 that discrete forcing does influence the growth of the vorticity field in the jet. Comparison of Figures 12(a) and 12(c) shows that, for this instant in time, the asymmetric

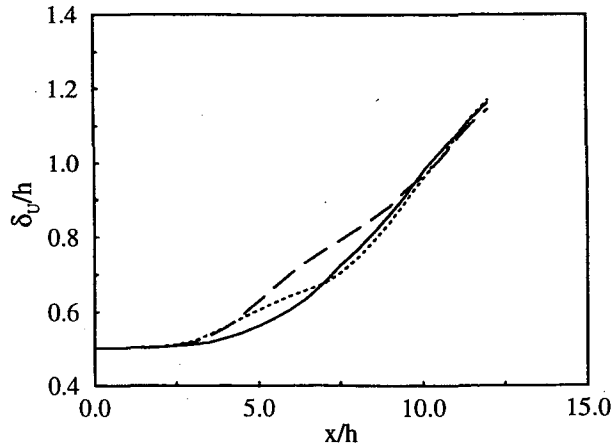


Figure 15: Downstream evolution of the jet half-width for discretely forced jets. — Unforced, ..... Symmetrically forced, -- Asymmetrically forced.

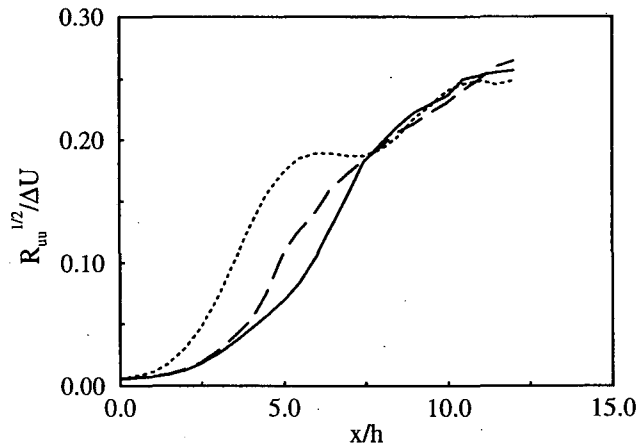


Figure 16: Downstream evolution of the centerline streamwise fluctuation intensity for forced jets. — Unforced, ..... Symmetrically forced, -- Asymmetrically forced.

forcing results in an increase in the downstream spread of the vorticity in the jet. This effect results in wider profiles, across the jet, of the turbulent kinetic energy and dissipation for the forced jets compared to the unforced jet. At  $x/h = 11.5$  the turbulent kinetic energy profiles, not shown, for the symmetrically and asymmetrically forced jets are 12% and 18% wider, respectively, than the profile for the unforced jet.

Figure 16 shows the downstream evolution of the streamwise Reynolds stress on the jet centerline for the two discretely forced jets as well as the unforced jet. It can be seen that symmetric forcing at the inflow dramatically increases the growth in the centerline longitudinal Reynolds stress. This is largely an effect of the enforced symmetry of the large-scale structures in the near field of the jet. The influence of the asymmetric forcing on the streamwise Reynolds stress is significantly smaller, although there is some impact in the region  $3.0h \leq x \leq 7.0h$ . Downstream, the centerline streamwise Reynolds stress for both of the discretely forced jets collapses to that of the unforced jet. There is no significant influence of discrete forcing on the downstream evolution of the streamwise Reynolds stress (not shown here) in the shear layers ( $y = \pm 0.5h$ ).

Figure 17 shows the downstream evolution of the lateral Reynolds stress on the jet centerline for the two discretely forced jets as well as the unforced jet. There is no significant impact of

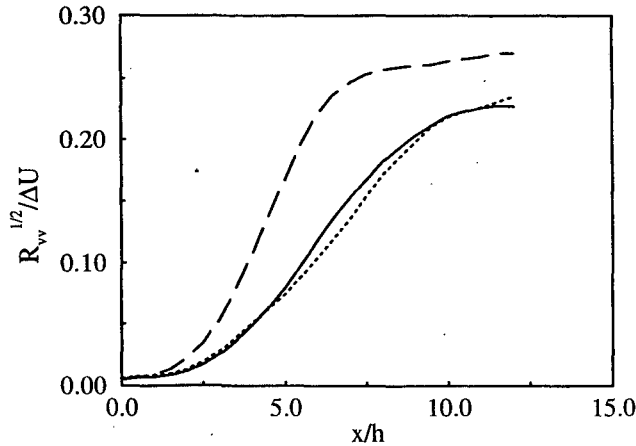


Figure 17: Downstream evolution of the centerline lateral fluctuation intensity for forced jets. — Unforced, ..... Symmetrically forced, - - - Asymmetrically forced.

symmetric discrete forcing on the evolution of the centerline lateral Reynolds stress due to the enforced symmetry of the large-scale structures. Symmetric large-scale structures do not impose lateral fluctuations at the centerline of the jet, therefore turbulent transport of the lateral Reynolds stress from the shear layers is still the dominant means by which the centerline values grow initially. Asymmetric forcing, however, does strongly increase the downstream growth in the lateral Reynolds stress. The asymmetric large-scale structures impose large lateral fluctuations at the centerline of the jet. The lateral Reynolds stress on the centerline for the asymmetrically forced jet peaks rapidly and remains relatively constant through the remainder of the domain. With the domain size used in these simulations, a relaxation of the lateral Reynolds stress in the asymmetrically jet back to the unforced values is not observed. In contrast to the streamwise Reynolds stress, both the symmetric and asymmetric forcing cause an increase in the downstream growth of the lateral Reynolds stress (not shown here) in the shear layers ( $y = \pm 0.5h$ ).

There is negligible influence of the symmetric forcing on the spanwise Reynolds stress and only a small influence of asymmetric forcing. This is a result of the two-dimensional nature of the discrete forcing used in this study. It is expected that some energy would transfer from the streamwise and lateral components of the Reynolds stress to the spanwise component through the pressure-strain terms. However, it appears this effect is small.

## 4 Conclusions

While the flowfield conditions in the shear layers at the nozzle of planar jets are seldom reported in detail, it is clear from the current results that they have a significant impact on the initial development,  $0.0 < x/h < 10.0$ , in these flows. Variations in the broadband fluctuation intensity in the shear layer as well as the shear layer momentum thickness significantly affect the rate at which the jet develops downstream. This is felt most strongly in the virtual origins of the jet half width and decay of the centerline velocity excess. Higher broadband fluctuation intensities or thinner shear layers lead to more rapidly developing jets with an asymptotic approach of the centerline turbulent kinetic energy to the self-similar values. Thicker shear layers or lower intensity inflow fluctuations result in an overshoot of the centerline turbulent kinetic energy. This overshoot is a result of the initial imbalance in the strong growth of the turbulent kinetic energy, through the production terms, and dissipation for these jets. The self-similar values downstream in the jet are reached when the appropriate balance between the production, dissipation and transport is achieved. The influence of

the shear layer thickness suggests that the initial development of the jet is dominated by the shear layer instabilities.

Two-dimensional discrete forcing at the inflow plane of planar turbulent jets has a significant impact on the initial development of the centerline streamwise and lateral Reynolds stresses. This influence, however, appears to be predominantly due to the enforced symmetry or asymmetry, as well as two-dimensionality, of the large-scale structures near the inflow. Symmetric forcing enhances the growth of the streamwise Reynolds stress with no impact on the lateral Reynolds stress while asymmetric forcing primarily affects the lateral Reynolds stress at the jet centerline. The two-dimensional discrete forcing has only a small affect on the downstream jet growth and centerline velocity decay as well as on the spanwise Reynolds stress. In general, discrete forcing, especially asymmetric forcing, enhances the growth and two-dimensionality of the large-scale structures near the jet nozzle, however, within the interior of the structures significant small-scale three-dimensionality is present. Downstream, these large-scale structures rapidly breakdown under the influence of the small-scale turbulence and the influence of the discrete forcing is felt only in the lateral Reynolds stress. The streamwise and spanwise Reynolds stresses as well as jet growth and centerline velocity decay rapidly collapse with those of the unforced jet downstream.

## 5 Acknowledgments

Support for the first author was provided by the Applied Mathematical Sciences Program of the DOE Office of Mathematics, Information, and Computational Sciences under contract DE-AC03-76SF00098 as well as by the Department of Energy Computational Sciences Graduate Fellowship Program. Partial support for the second author was provided by AFOSR through grant F49620-96-1-0106. This work was supported in part by a grant of HPC time from the Naval Oceanographic Office Department of Defense Major Shared Resource Center. In addition, this research used resources of the National Energy Research Scientific Computing Center, which is supported by the Office of Energy Research of the U.S. Department of Energy.

## References

- [1] Michalke, A. and Freymuth, P., "The Instability and the Formation of Vortices in a Free Boundary Layer," *Separated Flows, Part 2*, AGARD Conference Proceedings 4, Advisory Group for Aerospace Research and Development, 64 Rue De Varenne, Paris, France, May 1966, pp. 575-595.
- [2] Sato, H., "The Stability and Transition of a Two-Dimensional Jet," *J. Fluid Mech.*, Vol. 7, No. 1, 1960, pp. 53-80.
- [3] Rockwell, D. O. and Niccolls, W. O., "Natural Breakdown of Planar Jets," *Trans. ASME: J. Basic Engrg.*, Vol. 1, Dec. 1972, pp. 720-730.
- [4] Antonia, R. A., Browne, L. W. B., Rajagopalan, S., and Chambers, A. J., "On the Organized Motion of a Turbulent Plane Jet," *J. Fluid Mech.*, Vol. 134, 1983, pp. 49-66.
- [5] Bradbury, L. J. S., "The Structure of a Self-Preserving Turbulent Plane Jet," *J. Fluid Mech.*, Vol. 23, No. 1, 1965, pp. 31-64.
- [6] Gutmark, E. and Wynanski, I., "The Planar Turbulent Jet," *J. Fluid Mech.*, Vol. 73, No. 3, 1976, pp. 465-495.
- [7] Ramaprian, B. R. and Chandrasekhara, M. S., "LDA Measurements in Plane Turbulent Jets," *ASME J. Fluids Engrg.*, Vol. 107, Jun. 1985, pp. 264-271.

- [8] Oler, J. W. and Goldschmidt, V. W., "Interface Crossing Frequency as a Self-Preserving Flow Variable in a Turbulent Plane Jet," *Phys. Fluids*, Vol. 23, No. 1, Jan. 1980, pp. 19-21.
- [9] Oler, J. W. and Goldschmidt, V. W., "A Vortex-Street Model of the Flow in the Similarity Region of a Two-Dimensional Free Turbulent Jet," *J. Fluid Mech.*, Vol. 123, 1982, pp. 523-535.
- [10] Mumford, J. C., "The Structure of the Large Eddies in Fully Developed Turbulent Shear Flows. Part 1: The Plane Jet," *J. Fluid Mech.*, Vol. 118, 1982, pp. 241-268.
- [11] Thomas, F. O. and Goldschmidt, V. W., "Acoustically Induced Enhancement of Widening and Fluctuation Intensity in a Two-Dimensional Turbulent Jet," *ASME J. Fluids Engrg.*, Vol. 108, Sep. 1986, pp. 331-337.
- [12] Thomas, F. O. and Goldschmidt, V. W., "Structural Characteristics of a Developing Turbulent Planar Jet," *J. Fluid Mech.*, Vol. 163, 1986, pp. 227-256.
- [13] Thomas, F. O. and Chu, H. C., "An Experimental Investigation of the Transition of a Planar Jet: Subharmonic Suppression and Upstream Feedback," *Phys. Fluids A*, Vol. 1, No. 9, Sep. 1989, pp. 1566-1587.
- [14] Thomas, F. O. and Prakash, K. M. K., "An Experimental Investigation of the Natural Transition of an Untuned Planar Jet," *Phys. Fluids A*, Vol. 3, No. 1, Jan. 1991, pp. 90-105.
- [15] Namer, I. and Ötügen, M. V., "Velocity Measurements in a Plane Turbulent Air Jet at Moderate Reynolds Numbers," *Exp. Fluids*, Vol. 6, 1988, pp. 387-399.
- [16] Carpenter, M. H. and Kennedy, C. A., "Fourth-Order 2N-Storage Runge-Kutta Schemes," NASA Technical Memorandum 109112, National Aeronautics and Space Administration, Langley Research Center, Hampton, VA 23681, Jun. 1994.
- [17] Lele, S. K., "Compact Finite Difference Schemes with Spectral-like Resolution," *J. Comput. Phys.*, Vol. 103, 1992, pp. 16-42.
- [18] Carpenter, M. H., Gottlieb, D., and Abarbanel, S., "The Stability of Numerical Boundary Treatments for Compact High-Order Finite-Difference Schemes," *J. Comput. Phys.*, Vol. 108, 1993, pp. 272-295.
- [19] Thompson, K. W., "Time Dependent Boundary Conditions for Hyperbolic Systems," *J. Comput. Phys.*, Vol. 68, 1987, pp. 1-24.
- [20] Thompson, K. W., "Time-Dependent Boundary Conditions for Hyperbolic Systems II," *J. Comput. Phys.*, Vol. 89, 1990, pp. 439-461.
- [21] Rudy, D. H. and Strikwerda, J. C., "A Nonreflecting Outflow Boundary Condition for Subsonic Navier-Stokes Calculations," *J. Comput. Phys.*, Vol. 36, 1980, pp. 55-70.
- [22] Poinso, T. J. and Lele, S. K., "Boundary Conditions for Direct Simulations of Compressible Viscous Flows," *J. Comput. Phys.*, Vol. 101, 1992, pp. 104-129.
- [23] Hu, F. Q., "On Absorbing Boundary Conditions for Linearized Euler Equations by a Perfectly Matched Layer," *J. Comput. Physics*, Vol. 129, No. 1, Nov. 1996, pp. 201-219.
- [24] Browne, L. W. B., Antonia, R. A., Rajagopalan, S., and Chambers, A. J., "Interaction Region of a Two-Dimensional Turbulent Plane Jet in Still Air," *Structure of Complex Turbulent Shear Flow*, edited by R. Dumas and L. Fulachier, IUTAM Symp. Marseille 1982, Springer, 1983, pp. 411-419.



- [25] Hussain, A. K. M. F. and Clark, A. R., "Upstream Influence on the Near Field of a Plane Turbulent Jet," *Phys. Fluids*, Vol. 20, No. 9, Sep. 1977, pp. 1416-1426.
- [26] Stanley, S. A. and Sarkar, S., "A Study of the Flowfield Evolution and Mixing in a Planar Turbulent Jet Using Direct Numerical Simulation," *J. Fluid Mech.*, *in preparation*, 1999.
- [27] Stanley, S. A. and Sarkar, S., "Direct Numerical Simulation of the Developing Region of Turbulent Planar Jets," *AIAA Paper 99-0288*, 1999.

**ERNEST ORLANDO LAWRENCE BERKELEY NATIONAL LABORATORY  
ONE CYCLOTRON ROAD : BERKELEY, CALIFORNIA 94720**